



Universidad Autónoma
de Madrid

Biblos-e Archivo
Repositorio Institucional UAM

Repositorio Institucional de la Universidad Autónoma de Madrid
<https://repositorio.uam.es>

Esta es la **versión de autor** del artículo publicado en:
This is an **author produced version** of a paper published in:

Chemical Engineering Journal 309 (2017): 596-606

DOI: <https://doi.org/10.1016/j.cej.2016.10.002>

Copyright: © 2016 Elsevier Ltd. This manuscript version is made available under the CC-BY-NC-ND 4.0 licence <http://creativecommons.org/licenses/by-nc-nd/4.0/>

El acceso a la versión del editor puede requerir la suscripción del recurso
Access to the published version may require subscription

Degradation of emerging pollutants in water under solar irradiation using novel TiO₂-ZnO/clay nanoarchitectures

M. Tobajas, C. Belver*, J.J. Rodriguez

Seccion de Ingenieria Quimica, Facultad de Ciencias, Universidad Autonoma de Madrid, Campus Cantoblanco, Madrid E-28049, Spain

ARTICLE INFO

Article history:

Received 27 June 2016

Received in revised form 2 September 2016

Accepted 1 October 2016

Available online xxx

ABSTRACT

Emerging water pollutants, such as pharmaceuticals, are currently under study due to the increasing concern on the risks they pose on humans and the environment. Herein, solar photocatalytic technology is used for the degradation of model pharmaceuticals, including acetaminophen (ACE) and antipyrine (ANT), with novel TiO₂-ZnO/clay nanoarchitectures. These photocatalysts are based on the heterojunction between TiO₂-ZnO semiconductors and a delaminated layered clay. The structural, electronic and textural features of the photocatalysts were characterized by different techniques. The degradation rate has been checked under different conditions, including target compound and catalyst concentrations, intensity of the solar light and the combination of pharmaceuticals. ANT showed a higher degradation rate than ACE and in both cases the degradation was favored at low concentrations. The disappearance of both compounds was well described by a simple pseudo-first-order rate equation. Although both target compounds were almost completely removed, some TOC was still remaining corresponding to short-chain carboxylic acids and unidentified by-products with very low significance in terms of ecotoxicity. Scavengers were used to learn on the radical mechanism of the reaction and different behavior was observed for each target compound. The results of this study prove the ability and stability after several operation cycles of these novel photocatalysts to promote the degradation of these pollutants under solar light irradiation.

© 2016 Published by Elsevier Ltd.

1. Introduction

Nowadays a great variety of pharmaceuticals, pesticides, hormones and personal care products are often found in water and wastewaters. These compounds are named emerging contaminants and have drawn significant attention due to their potential environmental and health impact [1,2]. They are considered potentially hazardous since many of them are recognized endocrine disruptors and their release cannot be easily controlled because high quantities are used worldwide [3–5]. The removal efficiency of emerging contaminants through water treatment facilities varies from negligible to almost complete [6,7]. However, most pharmaceuticals are fairly resistant to chemical oxidation treatments and their toxicity hinders biological degradation [8] so that discharge into the environment represents a highly concerning problem.

Among those emerging contaminants, acetaminophen (ACE) is one of the most widely used analgesic and antipyretic drug. It is ranked as one of the top pharmaceuticals prescribed in USA [9] or England [10], being China the second ACE manufacturer [11]. The presence of this compound in water bodies is due in around 60–70% to human excretion via urine after consumption [12]. It has been detected in sewage treatment plant effluents as well as in surface water, where concentrations of 10–65 µg L⁻¹ have been found in US and Europe

[13–15]. This compound may lead to hepatic necrosis caused by its transformation to N-acetyl-p-benzoquinone-imine upon oxidation, which can hydrolyze to 1,4-benzoquinone, also a toxicant of major concern [16]. Other pharmaceutical detected in sewage effluents and surface water is antipyrine (ANT), a non-steroidal anti-inflammatory drug and antipyretic that also enters the environment after used and its accumulation can affect to aquatic life and cause adverse health effects, such as liver injury. A recent review of data on the concentrations of emerging contaminants in the influent and effluent from wastewater treatment plants showed that although the concentration of ANT was relatively low (0.04 mg L⁻¹), approximately 68.5% escaped from conventional activated sludge wastewater treatments, allowing it to reach surface water streams and distribute into the environment [17].

Biological treatment is nowadays considered to be among the best available technologies for wastewater treatment [18,19], but there are many pollutants that are toxic, chemically stable or resistant to biodegradation. In order to avoid undesired accumulation of pharmaceuticals in aquatic environments, technologies that enable efficient and safe removal of emerging pollutants from water have been developed and/or are being investigated. Among them, several advanced oxidation processes such as heterogeneous photocatalysis [20] and photo-Fenton [21,22] are gaining growing attention for the treatment of water containing pharmaceuticals [23,24]. A variety of semiconductors has been explored in modern photoassisted techniques, including metal oxides (TiO₂, ZnO, WO₃) and chalcogenides (CdS,

*Corresponding author.

Email address: carolina.belver@uam.es (C. Belver)

CdSe). Among them, TiO_2 is the most widely used due to their unique properties, such as high chemical stability, non-toxicity, biocompatibility and strong redox power [25,26]. Because of its large band gap (around 3.2 eV), UV radiation (<385 nm) can generate electron-hole pairs (e^-/h^+) that induce a series of reactions generating free-radicals capable of oxidizing the adsorbed pollutants [27]. However, these semiconductors usually show lower efficiency at low contaminant concentrations because of their small surface area and low adsorption capacity [28].

Continuous research efforts have been focussed on enhancing the photocatalytic performance of photocatalysts, aimed to improve the efficiency under visible light and reduce the e^-/h^+ recombination. Several strategies have been proposed to develop photocatalysts with visible activation, either by shifting the absorption edge, or by sensitizing TiO_2 with surface additives [29]. Nevertheless, other efforts have been focused on the synthesis of coupled semiconductor- TiO_2 photocatalysts, such as ZnO -, WO_3 -, Cu_2O -, CdS - or BiOxCl - [29,30]. The synthesized couples create heterojunctions that enhances the photocatalytic efficiency by decreasing the recombination rate of the photo-generated e^-/h^+ pairs. These heterojunctions can compensate the disadvantages of the individual components, and induce a synergistic effect like an efficient charge separation [31]. In this field, some recent works report the synthesis of several TiO_2 - ZnO couples, such as composite spheres [32], ZnO nanorods covered by TiO_2 [33] or photonic crystals [34] by using different synthesis procedures.

The efforts devoted to obtain efficient photocatalysts also aimed to use nanosized semiconductors, because the quantum size effect yields superior photocatalytic performances due to their large surface area and good dispersion capability [35]. Nevertheless, nanosized photocatalysts tend to aggregate in suspension, resulting in a loss of photo-efficiency and hindering the separation and recovery of the photocatalyst. These matters lead to key obstacles for industrial applications, and cause a considerable increase in operation costs [36,37]. To resolve these issues, recent strategies have been addressed by creating porous photocatalyst networks or assembling nanostructured photocatalysts on porous supports. In this sense, novel methodologies have been developed to control the morphological and structural properties of the semiconductors. Highlighting, the creation of multi-dimensional (0D, 1D, 2D, and 3D) TiO_2 -based materials [29,38] or microsphere photocatalysts based on doped- TiO_2 , ZnO , Bi_2WO_6 , BiOX ($X = \text{Cl}, \text{Br}, \text{I}$), among others, appearing as an interesting alternative for photocatalyst recovery and reuse [39].

Because the interest on facilitating the recovering of the photocatalyst while maintaining its photocatalytic efficiency, searching for new strategies to assemble nanostructured semiconductors on porous supports has been also pursued in photocatalysis. Different porous solids have been employed to prepare TiO_2 -based photocatalysts, including mesoporous silica, clays, zeolites, activated carbon or glass spheres [35,40]. Clay minerals have been extensively used as supports in heterogeneous catalysis because of their surface area, layered or fibrous structure and high adsorption capacities. TiO_2 -pillared clays have been from long time the most studied clay-based materials in photocatalysis, combining the adsorption capacity of the clay and the photocatalytic ability of TiO_2 [41,42]. These materials are characterized by a high surface area and a porous network, mainly integrated by micropores, due to the creation of oxide pillars anchored to the layers of a layered clay [43]. Nevertheless, recent advances have been reported in the synthesis and photocatalytic applications of clay-based photocatalysts, focusing the attention on using the photocatalysts under the visible-light irradiation. Several reviews report the synthesis of new clay-based materials by sol-gel, hydrothermal and solution mixing methods [40,44]. It has been described the assembling

of different semiconductors (TiO_2 , ZnO , CdS , Ag/AgBr , Bi_2WO_6) on the surface of different clay minerals, with layered (montmorillonite) and fibrous structures (sepiolite, halloysite). Moreover, other derived-clay materials with large surface area can be also prepared from layered clays by incorporating metal oxide nanoparticles into the interlayered space, yielding its delamination and making accessible the inner surface of the clay layers. This methodology leads to metal oxide/clay nanoarchitectures with a porous structure integrated by micro- and mesopores [45,46]. These kind of nanoarchitectures have been prepared by a modified sol-gel methodology that consists on the hydrolysis and polycondensation of metal alkoxides inside the interlayer space of clays, opening the layered structure of the clay and making accessible both the internal and external surface of the layers.

Thus, the aim of this work was to synthesize active photocatalysts for the degradation under solar light irradiation of two widely used pharmaceuticals, acetaminophen and antipyrine, taken as model emerging pollutants. To prepare the novel nanoarchitectures the modified sol-gel route mentioned before was followed [45,47], adapting the experimental conditions to obtain for the first time, nanostructured TiO_2 - ZnO supported on a delaminated layered clay. The purpose was to construct novel photocatalysts based on semiconductor-semiconductor (S-S) heterojunctions assembling on a delaminated clay. Although TiO_2 and ZnO have similar band gap values, it has been described that the heterojunction between different semiconductors can enhance their photocatalytic activity, because it can reduce the probability of electron-hole recombination and promote the migration of photogenerated carriers [30]. The optimal working conditions relative to initial concentration of target compound, catalyst loading and light intensity were tested for the sake of learning on the potential application. The rate of disappearance of the two pharmaceuticals tested was determined individually and in mixtures. Experiments with radical scavengers were carried out to learn on the mechanism of the photocatalytic process.

2. Experimental

2.1. Materials

Cloisite®30B (from now named cloisite) was selected as pristine organoclay, supplied by Southern Clay Products, to synthesize the nanoarchitectures, characterized by a layered structure. Titanium (IV) isopropoxide ($\text{Ti}(\text{IPO})$, $>97\%$ Sigma Aldrich), zinc acetate dihydrate ($\text{Zn}(\text{acet})$ $>98\%$ Sigma Aldrich) and isopropanol (iPrOH , Panreac) were also used for the synthesis. Acetaminophen (ACE) ($>99\%$ Sigma Aldrich) and antipyrine (ANT) (phenazone, 99% Sigma Aldrich) were selected as target compounds for testing the photocatalytic activity. Their respective chemical formulas are included in Schemes S2 and S3 of ESI. Acetonitrile (Panreac) and formic acid ($>95\%$ Sigma Aldrich) were used to prepare the mobile phase for liquid chromatography. KI (Fluka), isopropanol (Panreac) and 1,4-benzoquinone (BQ, Sigma Aldrich) were used as radical scavengers for the elucidation of the reaction mechanism.

2.2. Synthesis of TiO_2 - ZnO /cloisite photocatalysts

TiO_2 - ZnO /cloisite photocatalysts were synthesized following a modified sol-gel procedure described for other nanoarchitectures [45,48]. Cloisite (1 g) was dispersed in iPrOH (10 w/w%) under stirring for 48 h to achieve a homogenous dispersion. Afterwards, a volume of $\text{Ti}(\text{IPO})$ in iPrOH (70 v/v%) was added to the dispersion at 50°C , using a TiO_2 /clay ratio of 2/1. Then, an aqueous solution formed by $\text{Zn}(\text{acet})$ /water/ iPrOH was slowly added, using different $\text{Zn}(\text{acet})$ amounts to achieve ZnO/TiO_2 ratios (w/w%) equal to 0, 0.2,

0.5, 1, 2 and 5%. The amount of water was the stoichiometric for hydrolyzing the TiIPO , and the $i\text{PrOH}$ amount (used as solvent) was calculated to have a 50 v/v% $i\text{PrOH}$ /water ratio. The mixture was maintained under stirring at 50 °C until the formation of a white gel, needing time intervals lower than 30 min. The resulting gel was dried at 50 °C and then heated up to 500 °C for 4 h in air to burn-out the organic species used during the synthesis. The final solids were named according to the ZnO percentage, being TiO_2/cloi , $\text{TiO}_2\text{-}0.2\text{ZnO}/\text{cloi}$, $\text{TiO}_2\text{-}0.5\text{ZnO}/\text{cloi}$, $\text{TiO}_2\text{-}1.0\text{ZnO}/\text{cloi}$, $\text{TiO}_2\text{-}2.0\text{ZnO}/\text{cloi}$ and $\text{TiO}_2\text{-}5.0\text{ZnO}/\text{cloi}$. Other catalysts series were prepared with higher ZnO percentages (from 10 to 50%) but they were dismissed because the addition of higher amounts of $\text{Zn}(\text{acet})$ precursor destabilized the colloidal dispersion giving rise to a non-homogeneous gel. The ZnO/cloi sample was not successfully obtained by this methodology because it requires an alkoxide precursor of Zn that is not commercially available.

2.3. Characterization of the photocatalysts

The $\text{TiO}_2\text{-ZnO}/\text{cloisite}$ photocatalysts were characterized by several techniques. X-ray diffraction (XRD) spectra were obtained in an X-ray Bruker D8 diffractometer equipped with a Sol-X energy detector, using $\text{Cu K}\alpha$ radiation and recording a 2θ range equal to $2\text{--}70^\circ$ with a scanning rate of $1.5^\circ/\text{min}$. UV-vis diffuse reflectance spectra (DRS) were recorded by a Shimadzu 2501PC UV-vis spectrophotometer from 300 to 900 nm, using BaSO_4 as a reference material. The band gap values were estimated using the Tauc Plot standard technique [49], considering indirect semiconductors like TiO_2 [50]. Plotting $(F(R) \times h\nu)^{1/2}$ versus $h\nu$ (eV) yields a graph with a linear region whose extrapolation to x axis provides the band gap value. A Micromeritics Tristar 123 analyzer was used for the textural characterization by N_2 adsorption-desorption at -196°C . The BET surface area (S_{BET}) was determined by the BET method, the internal (S_{INT}) and the external surface areas (S_{EXT}) were calculated by the t-plot method of De Boer, and the total pore volume (V_T) from the amount of N_2 adsorbed at a relative pressure of 0.99. The samples were previously outgassed at 150 °C overnight in a Florprep 060 Micromeritics device. Field emission scanning electron microscope (SEM) images were registered using a FEI microscope (NOVA NANOSEM 230) and transmission electron microscope (TEM) images were obtained with a TEM 200 kV, Tecnai G220 from FEI COMPANY at an accelerating voltage of 200 kV.

2.4. Evaluation of the photocatalytic activity

The photocatalytic reactions were performed in a glass (Pyrex) batch slurry reactor under simulated solar light. Aqueous solutions (300 mL) with different initial concentrations of the target compounds were mixed with different amounts of the synthesized photocatalysts. The reactor was sealed with a top cover with two ports for sampling and air inlet (50 mL min^{-1} flow rate). The dispersion was left under stirring in dark overnight (18 h) to disperse the catalyst and to achieve the complete adsorption equilibrium. The reactor was located in the interior of a solar simulator (Suntest XLS+, from ATLAS) equipped with a Xe lamp and a Solar ID65 filter that cuts off the UV light contribution at 320 nm, which simulates solar radiation. The Suntest system allowed changing the intensity of irradiation, which was varied between 250 and 650 W m^{-2} . The solar simulator has several fans for cooling the interior, maintaining the temperature at $38 \pm 1^\circ\text{C}$. After the adsorption time, the light was switched on and 8 mL aliquots were withdrawn at different time intervals. These samples were filtered through $0.45\text{ }\mu\text{m}$ syringe filters (Teknokroma)

to remove the catalyst powder. For the most active synthesized photocatalyst, the effect of acetaminophen concentration ($4\text{--}35\text{ mg L}^{-1}$) and catalyst dosage ($50\text{--}500\text{ mg L}^{-1}$) was studied. The experiments were conducted in triplicate.

2.5. Analytical methods

ACE and ANT were analyzed by HPLC (Varian ProStart 410) equipped with a UV-visible detector (ProStart 325) and a reversed phase C18 column (luna, Phenomenex). The mobile phase was a mixture of acetonitrile:formic acid (0.1 v/v% in water) using a gradient method (10:90%–40:60% (0–16 min)) with a flow rate of 0.35 mL min^{-1} . Two different wavelengths were set for the detection of antipyrine and acetaminophen (256 and 246 nm, respectively). In these conditions, antipyrine appeared at retention time of 12 min while acetaminophen was detected at 5.6 min. The total organic carbon (TOC) of the samples was measured by a Shimadzu TOC equipment. Short-chain carboxylic acids (formic, acetic, malonic and oxalic acids) were measured by ionic chromatography using a Metrohm 790 Personal IC equipment. Ecotoxicity tests were performed using a Microtox M500 Analyzer (Azur Environmental) following the standard Microtox test procedure (ISO 11348-3, 1998), based on the reduction of the light emission by the marine bacteria *Vibrio fischeri*. The ecotoxicity was expressed as toxicity units (TU) as the inverse ratio to IC_{50} values. The experiments with radical scavengers were carried out under the same experimental conditions described for the photocatalytic reactions. KI, $i\text{PrOH}$ and BQ were introduced in the target solution at 0.001 M concentration prior to the addition of the catalyst.

3. Results and discussion

3.1. Characterization of the photocatalysts

Fig. 1 and Fig. S1A of ESI show the XRD patterns of cloisite and $\text{TiO}_2\text{-ZnO}/\text{cloisite}$ with different ratios of ZnO and TiO_2 . The diffractograms show the peaks of TiO_2 corresponding to the tetragonal anatase phase (JCPDS n°. 78-2486), indicating that the incorporation of low ZnO loading (below 5%) does not prevent the crystallization of anatase. The crystal size of the anatase phase was estimated by the Scherrer's equation, resulting in similar values for all nanoarchitectures, ca. to 13 nm. However, as mentioned before, the synthesis of nanoarchitectures with higher ZnO loading (from 10 to 50%) did not

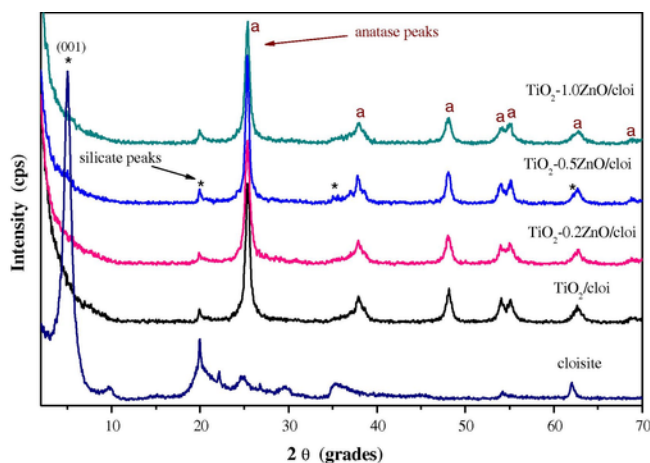


Fig. 1. XRD diffractograms of cloisite and the $\text{TiO}_2\text{-ZnO}/\text{cloisite}$ with different ratios of ZnO and TiO_2 .

work out well, resulting in non-homogeneous solids whose XRD patterns did not show the formation of the desired anatase phase (depicted in Fig. S1B). From Fig. 1 and Fig. S1A, it can be also seen that, comparing the nanoarchitectures with the pristine organoclay, the characteristic (0 0 1) peak ($2\theta = 4.85^\circ$) of the layered clay has disappeared in all cases regardless of the ZnO amount. This indicates that the layered clay has lost its ordered structure because of TiO_2 -ZnO incorporation at low percentages. However, the other reflections of the organoclay remained unchanged, indicating that although the clay layers are disordered they maintain their structural layer identity. So, the final TiO_2 -ZnO/cloisite catalysts result in a delaminated-clay material with the TiO_2 -ZnO phase located at the surface. This kind of structures have been described in previous works related with the preparation of metal doped- TiO_2 /clay heterostructures [45,47]. It is also important to note that no other unassigned peak appears in these XRD patterns. This fact apparently means that no other zinc or titanium phases crystallized during the synthesis, although, it is also possible that the crystallinity of other zinc phases was too poor for detection by XRD, considering the low amount of zinc incorporated during the synthesis.

The textural characteristics of the catalysts were assessed from the nitrogen adsorption-desorption isotherms at 77 K, and the corresponding results are summarized in Table 1. The TiO_2 /cloi gave a BET area of $233 \text{ m}^2 \text{ g}^{-1}$ while TiO_2 -ZnO/cloi heterostructures yielded

Table 1
Textural characteristics and band gap values of TiO_2 -ZnO/cloisite nanoarchitectures.

Catalyst	S_{BET} ($\text{m}^2 \text{ g}^{-1}$)	S_{EXT}^* ($\text{m}^2 \text{ g}^{-1}$)	V_T ($\text{cm}^3 \text{ g}^{-1}$)	Band gap energy (eV)
TiO_2 /cloi	233	124	0.262	3.19
TiO_2 -0.2ZnO/cloi	168	113	0.297	3.21
TiO_2 -0.5ZnO/cloi	165	109	0.251	3.25
TiO_2 -1.0ZnO/cloi	163	103	0.221	3.24
TiO_2 -2.0ZnO/cloi	164	110	0.210	3.21
TiO_2 -5.0ZnO/cloi	158	119	0.226	3.22

* S_{EXT} External or non-microporous area.

lower values (ca. $160 \text{ m}^2 \text{ g}^{-1}$) mainly due to frankly lower internal surface area. This reduction indicates that the incorporation of ZnO causes a detrimental effect on the textural characteristics of the nanoarchitectures, even at low ZnO loading. This effect can be related to the sol-gel transition that occurred during the synthesis that depends on the pH of the medium because of the hydrolysis step accelerates under acid conditions. Thus, in our case, the Zn(acet) used as precursor provides certain acidity that reduces the time for the gel formation and results in a faster formation of the TiO_2 precursor [51]. This precursor can partially block the access to the porous structure of the cloisite, yielding materials with lower microporosity and surface area. Nevertheless, the total pore volume of all nanoarchitectures was quite similar, due to the mesopore network that usually characterizes to layered-clay materials, mainly depending on the amount and nature of the clay [52,53].

Since the initial characterization of the catalysts indicated that the properties of the TiO_2 -ZnO/cloisite nanoarchitectures were similar regardless the amount of ZnO incorporated, we carried out a preliminary photocatalytic tests to study the effect of ZnO. Fig. S2 shows the photocatalytic degradation of ANT with the TiO_2 -ZnO/cloisite nanoarchitectures under solar light. It can be seen that the best activity performance is described by the catalysts with lower amount of ZnO incorporated, even the catalysts TiO_2 -2.0ZnO/cloi and TiO_2 -5.0ZnO/cloi showed lower activity than the catalyst based on only TiO_2 (TiO_2 /cloi). Therefore, we selected TiO_2 -0.2ZnO/cloi and TiO_2 -0.5ZnO/cloi as catalysts for further studies in order to consume less semiconductor amount.

The UV-vis DRS spectra of the TiO_2 -ZnO/cloisite nanoarchitectures and their Tauc plots are depicted in Fig. 2. All the nanoarchitectures synthesized show quiet similar light absorption profiles, with an absorption edge at 390 nm, typical of TiO_2 and ZnO phases [54,55]. The band gap energies were calculated by the Tauc Plot method [49], considering that these materials were indirect semiconductors [50] and following the equation: $\alpha h\nu \propto A (h\nu - E_g)^{1/2}$, being α , h , ν , E_g and A the absorption coefficient, Planck constant, radiation frequency, band gap and a constant, respectively [56]. According to

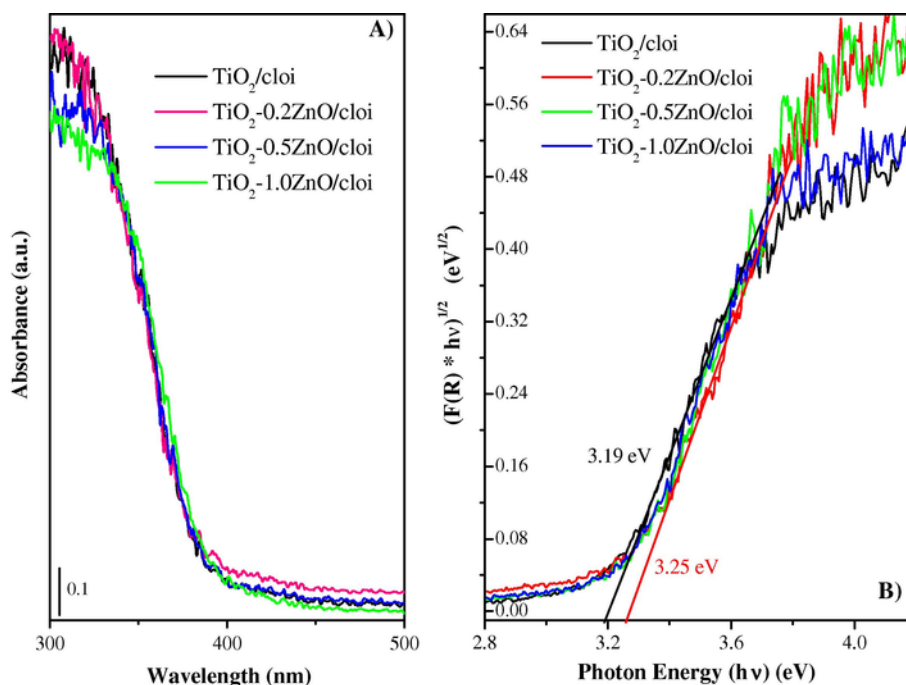


Fig. 2. UV-vis DRS spectra (A) and Tauc plots (B) of the TiO_2 -ZnO/cloisite nanoarchitectures.

this equation, a plot of $(\alpha h\nu)^{1/2}$ versus $h\nu$ (eV) was built, presented in Fig. 2B. The interception of the steep linear branch of these curves to the X axis provides approximate values of the band gap energies (included in Table 1). As can be seen, all the nanoarchitectures have similar band gap energies, close to 3.2 eV, regardless of ZnO loading. This result was expected because of both TiO_2 and ZnO have similar band edge (3.2 eV) [26], so their anchorage over the surface of a delaminated-layered clay should not cause modification on the electronic properties. The purpose of this work is synthesizing novel photocatalysts based on semiconductor-semiconductor (S-S) heterojunction (see Scheme S1 of ESI) rather than reducing the band gap of TiO_2 . Although TiO_2 and ZnO have similar band gap values, it has been described that the heterojunction between different semiconductors can enhance their photocatalytic activity. However, that improvement is not caused by the band gap shift to visible region, but because the heterojunction can reduce the probability of electron-hole recombination and promote the migration of photogenerated carriers [30].

Some representative FE-SEM images of the TiO_2 -0.5ZnO/cloi are shown in Fig. 3(A and B). These nanoarchitectures characterizes by a spongy morphology with the layered clay covered by the TiO_2 -ZnO particles, similar to previous titania nanoarchitectures [45,47]. The presence of these particles is more evident in the transmission electron micrographs depicted in Fig. 3(C and D). It can be seen that the TiO_2 -0.5ZnO particles are dispersed over the delaminated clay with sizes in the range between 10 and 20 nm. There are not notable differences between the nanoarchitectures depending on the ZnO incorporated. Its incorporation, at low concentrations, does not modify the

morphology of the nanoarchitecture and maintain the titania nanoparticles anchored over the delaminated layered clay.

3.2. Solar photocatalytic degradation of acetaminophen

3.2.1. Effect of ZnO content

The photocatalytic activity of the nanoarchitectures (TiO_2 /cloi, TiO_2 -0.2ZnO/cloi and TiO_2 -0.5ZnO/cloi) was evaluated in the degradation of ACE and ANT in aqueous solutions under solar light. Prior to the photocatalytic experiments, the adsorption capacity of these materials was checked in dark, showing a low adsorption towards the two pharmaceuticals tested. These results were further used to adjust the initial concentration of the target compound in each photocatalytic test. Firstly, experiments were carried out with 15 mg L^{-1} of target pollutant, 250 mg L^{-1} of catalyst and 450 Wm^{-2} of light intensity. The results obtained are shown in Fig. 4 that includes experiments in absence of photocatalyst with each compound, where it can be seen their stability under solar irradiation so that non-catalytic photolysis can be neglected. Around 70% of ACE was degraded after 600 min with the TiO_2 -0.5ZnO/cloi photocatalyst (Fig. 4A), showing higher photocatalytic activity than TiO_2 /cloi and TiO_2 -0.2ZnO/cloi. Similar results were found for ANT (Fig. 4B), with slightly higher conversion values. The photocatalytic activity of TiO_2 -0.5ZnO/cloi can be attributed to its higher ZnO content. Although the band edge values of all the photocatalysts were very similar, as indicated before, the heterojunction between TiO_2 -0.5ZnO favours the separation of photogenerated charges, avoiding recombination and enhancing the

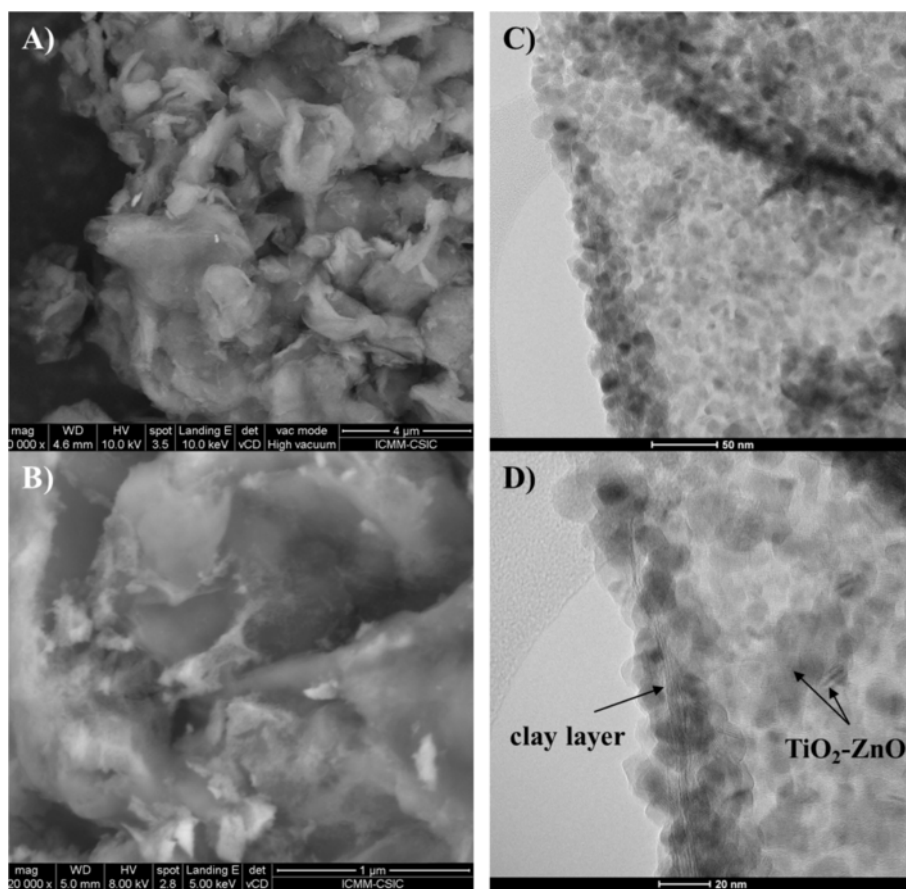


Fig. 3. FE-SEM images (A and B) and TEM images (C and D) of the TiO_2 -0.5ZnO/cloi catalyst.

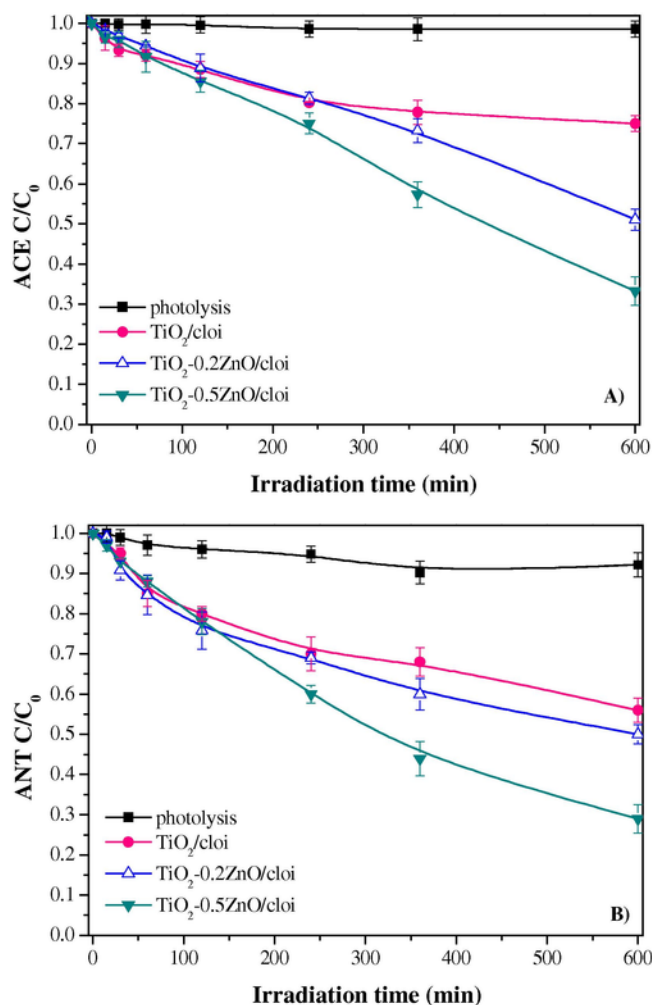


Fig. 4. Photocatalytic degradation of ACE (A) and ANT (B) with the $\text{TiO}_2\text{-ZnO/cloisite}$ nanoarchitectures under solar light ($[\text{pollutant}]_0 = 15 \text{ mg L}^{-1}$; $[\text{photocatalyst}] = 250 \text{ mg L}^{-1}$; irradiation intensity: 450 W m^{-2} ; three separate experiments were performed to estimate the error bars).

photoefficiency of these nanoarchitectures [62]. Therefore, this photocatalyst was used for further analysis of the operating conditions.

3.2.2. Effect of photocatalyst and initial ACE concentrations

The experiments for this purpose were carried out with ACE. Fig. 5 displays both effects, showing the conversion values after 6 h of irradiation at different catalyst and ACE concentrations. The respective evolution of the ACE concentration upon reaction time is given in Fig. S3 of ESI. From these results, it can be seen nearly complete conversion after 10 h and more than 90% after 6 h with catalyst loadings between 250 and 500 mg L^{-1} . Although high catalyst concentrations can lead to a reduction of light transmission and, subsequently, of degradation efficiency [11,57], we have not reached that situation in our experiments. Fig. 5 also shows the effect of varying ACE initial concentration (from 4 to 35 mg L^{-1}) at different catalyst loadings (the respective plots of ACE evolution versus irradiation time and the kinetic constants resulted by fitting to pseudo-first-order rate equation are shown in Fig. S4 of ESI). Except at the lowest catalyst loading, the highest ACE conversion values were obtained when working at 10 mg L^{-1} initial concentration and decreased significantly beyond that concentration. At 10 mg L^{-1} initial concentration ACE removal was quite similar with the catalyst at 250 and 500 mg L^{-1} ; then we selected the lowest one for further studies.

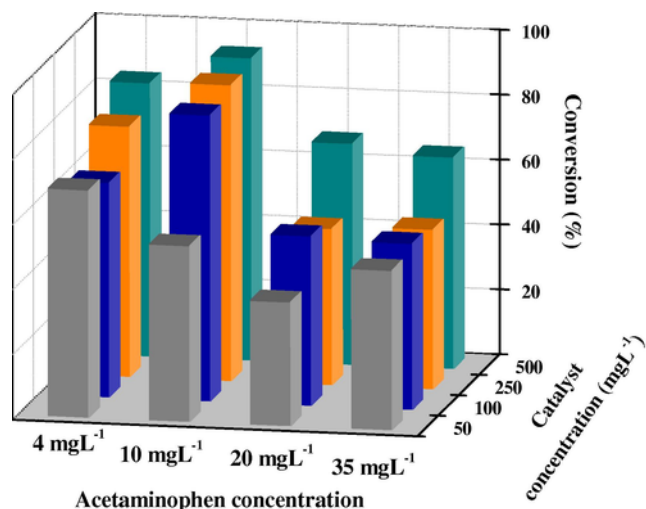


Fig. 5. Effect of catalyst and ACE initial concentration on ACE conversion with $\text{TiO}_2\text{-0.5ZnO/cloi}$ after 6 h under solar light (450 W m^{-2}).

3.2.3. Effect of the irradiation intensity

The evolution of ACE and ANT concentrations upon reaction time at different irradiation intensities is shown in Fig. 6. Increasing the intensity within the range tested ($250\text{--}450 \text{ W m}^{-2}$) increases the rate of disappearance of both compounds, consistently with the higher availability of photons to activate the photocatalyst and generate radicals. After 10 h of irradiation complete conversion was achieved at the highest intensity and more than 95% at 450 W m^{-2} . The degradation curves of Fig. 6 were fitted to a pseudo-first-order rate equation and the resulting kinetic constants are collected in Table 2. To evaluate the effect of light in more detail, the photonic efficiency (ξ) for each reaction experiment was estimated by the method described by Serpone [58], normalizing the kinetic constants by the photon flux calculated at each irradiation intensity. The values are included in Table 2. For ACE degradation a maximum value of $1.1 \text{ einstein}^{-1}$ was obtained at 450 W m^{-2} while the photonic efficiency yielded values close to $1.3\text{--}1.4 \text{ einstein}^{-1}$ for ANT degradation. It is noteworthy that the photonic efficiency shows fairly close values independently of the irradiation intensity within the range tested (with the exception of ACE at 250 W m^{-2}). Thus, this heterostructure performs efficiently as photocatalyst within a wide range of solar light intensity.

3.2.4. Photodegradation of a mixture of acetaminophen and antipyrine and recycling tests

A complementary study was performed with a mixture of ACE and ANT, for the sake of comparing the results with those obtained with the individual compounds separately. This experiment was carried out using 10 mg L^{-1} of each target compound. The evolution of both pollutants upon the irradiation time is shown in Fig. S5 of ESI, while the values of conversion after 6 h and the pseudo-first-order rate constant are summarized in Table 3. These values decreased with respect to the obtained individually but while that increase was of low significance in the case of ACE a more pronounced effect was observed for ANT. However, complete conversion was achieved after 10 h for both contaminants as in the separate experiments. To learn on the stability of the nanoarchitecture catalyst synthesized, its performance was checked upon sequence of light irradiation –dark –light irradiation steps of 5 h–15 h–5 h. The results (Fig. S6 of ESI) demonstrated that ACE and ANT were completely degraded after two

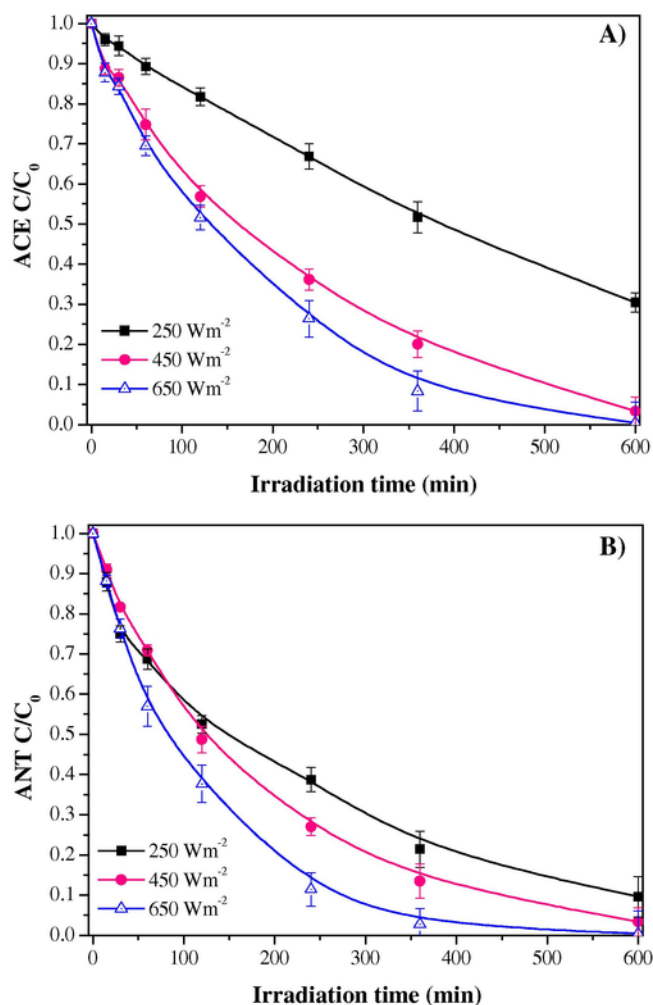


Fig. 6. Evolution of the ACE (A) and ANT (B) concentration upon time under solar irradiation at different intensities with the $\text{TiO}_2\text{-0.5ZnO/cloi}$ photocatalyst: $[\text{pollutant}]_0 = 10 \text{ mg L}^{-1}$; $[\text{photocatalyst}] = 250 \text{ mg L}^{-1}$; three separate experiments were performed to estimate the error bars).

5 h-cycles of solar light irradiation. Because the reusability of the photocatalyst is an important factor to take into account for practical applications, further reutilization tests were carried out maintaining the optimum conditions obtained in the previously described reactions, and using the same catalyst ($\text{TiO}_2\text{-0.5ZnO/cloi}$) during four cycles. Before each run, the catalyst was thoroughly washed with water and dried overnight at 100°C . The photodegradation percentage of ACE and ANT for the four successive 6 h of irradiation cycles is shown in Fig. 7. As can be seen the reused photocatalyst yield a decrease of only 15% of ANT conversion and 13% of ACE conversion with respect to the first cycle. This slight decrease in the photocatalytic activity after four cycles can be ascribed to the loss of photo-

catalyst during washing step. These results support the stability of the photocatalyst in the reaction conditions employed in this study.

3.2.5. TOC reduction and degradation by-products

The photocatalytic degradation of ACE and ANT was also followed through the evolution of TOC. The results are shown in Fig. 8. As can be seen, the disappearance of the starting compounds was not accompanied by a similar TOC reduction. In fact, less than 50% mineralization was achieved after 10 h of irradiation when complete conversion of ACE and ANT had been reached. The trend of the TOC curves clearly indicates that significant amounts of reaction by-products are refractory to the treatment investigated. The ANT degradation pathway has been reported for photoassisted AOPs [22,59], starting with the cleavage of the N-N bond of the penta-heterocycle that results in the formation of aromatic acids. Then, the phenyl ring is opened leading to the formation of short-chain carboxylic acids that finally may be partially oxidized to CO_2 . In our case, the by-products detected were small carboxylic acids, mainly acetic, formic and malonic and lesser amounts of oxalic. The evolution of these acids upon irradiation time is shown in Fig. 9A. Malonic acid was formed since the first steps of the process and was further degraded, whereas the curves of the shorter carboxylic acids show a continuous rising trend, particularly pronounced in the case of acetate. Following the degradation pathway described in the literature (Scheme S2 of ESI), we investigated the presence of anthranilic and terephthalic acids. We only detected the second but in very small concentration (0.07 mg L^{-1} at the most after 360 min of reaction). Fig. 9B represents the evolution of measured TOC, ANT, carboxylic acids and the non-identified by-products in equivalent carbon. It is noteworthy that the amount of these last increased upon reaction time up to a maximum somewhere between 4 and 6 h and then decreased to a value corresponding to the 25% of the equivalent C in the starting ANT. To learn more on the remaining TOC, we determined the ecotoxicity of the samples along the reaction time. The values are included in Fig. 9B as toxicity units (TU). The ecotoxicity slightly increased during the first 4 h but decrease to very low values, inferior to the starting ANT, after 6 h. Thus, although complete mineralization of antipyrine was not achieved after 10 h of solar irradiation with the catalyst tested the ecotoxicity was considerably reduced and the reaction by-products were less toxic than the parent compound.

With regard to ACE, it has been described that its photocatalytic degradation starts with the preferential addition of $\cdot\text{OH}$ at the ortho and para positions of the aromatic ring, yielding to different aromatic intermediate compounds that are further oxidized to carboxylic acids [60,61]. Between the aromatics compounds, it has been described the presence of hydroquinone, benzoquinone, trihydroxybenzene and *p*-nitrophenol (see Scheme S3 of ESI). Following that information, we investigated the formation of these aromatic by-products but only detected very small amounts of benzoquinone after 240 min of reaction, reaching a concentration lower than 0.1 mg L^{-1} . We also analyzed carboxylic acids, which were the same that those from ANT and their evolution upon reaction time showed a similar trend, except for malonic which appeared more resistant to degradation (Fig. 10A). So far we do not have a comprehensive explanation for this experimental ob-

Table 2

Values of the rate constant (k) and photonic efficiency (ξ) for ACE and ANT degradation at different irradiation intensities with $\text{TiO}_2\text{-0.5ZnO/cloi}$ photocatalyst.

	Acetaminophen			Antipyrine		
	250 Wm^{-2}	450 Wm^{-2}	650 Wm^{-2}	250 Wm^{-2}	450 Wm^{-2}	650 Wm^{-2}
$k \times 10^3 \text{ (min}^{-1}\text{)}$	1.9	5.4	6.6	3.8	5.6	9.2
$\xi \text{ (einstein}^{-1}\text{)}$	0.7	1.1	1.0	1.4	1.2	1.3

Table 3

Values of the rate constant and conversion at 6 h for ACE and ANT degradation, individually and mixed, using $\text{TiO}_2\text{-0.5ZnO/cloi}$ photocatalyst ($[\text{ACE}]_0 = 10 \text{ mg L}^{-1}$; $[\text{ANT}]_0 = 10 \text{ mg L}^{-1}$ [photocatalyst] = 250 mg L^{-1} , light intensity = 650 W m^{-2}).

	ACE-mixed	ACE	ANT-mixed	ANT
$k \times 10^3 \text{ (min}^{-1}\text{)}$	5.7	6.6	4.7	9.2
Conversion at 6 h (%)	88.3	91.4	82.3	97.2

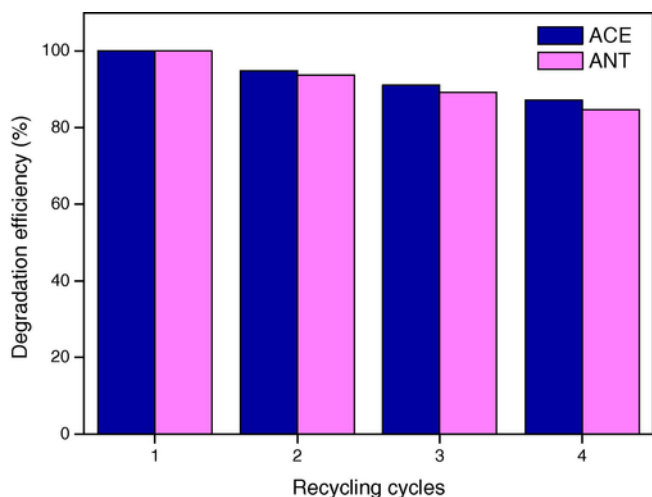


Fig. 7. Recycling tests of $\text{TiO}_2\text{-0.5ZnO/cloi}$ for the degradation of ACE (10 mg L^{-1}) and ANT (10 mg L^{-1}) during four successive cycles.

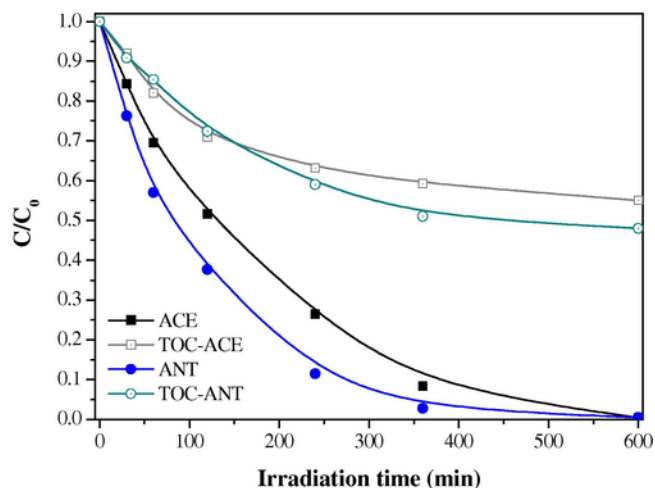


Fig. 8. Evolution of TOC in the photodegradation of ACE and ANT under solar light with the $\text{TiO}_2\text{-0.5ZnO/cloi}$ catalyst ($[\text{ACE}]_0 = [\text{ANT}]_0 = 10 \text{ mg L}^{-1}$; [photocatalyst] = 250 mg L^{-1} , irradiation intensity = 650 W m^{-2}).

servation but it might be related to some different behavior of the catalyst due to deactivation caused by some species from ACE degradation. Fig. 10B shows the carbon balance as in the case of ANT. Now, the TOC corresponding to non-identified species is lower during the first 4 h but follows a similar trend upon reaction time. The ecotoxicity of these samples from reaction was also determined (Fig. 10B) and it is important to remark the dramatic decrease of the toxicity units, which means the corresponding decrease of ecotoxicity.

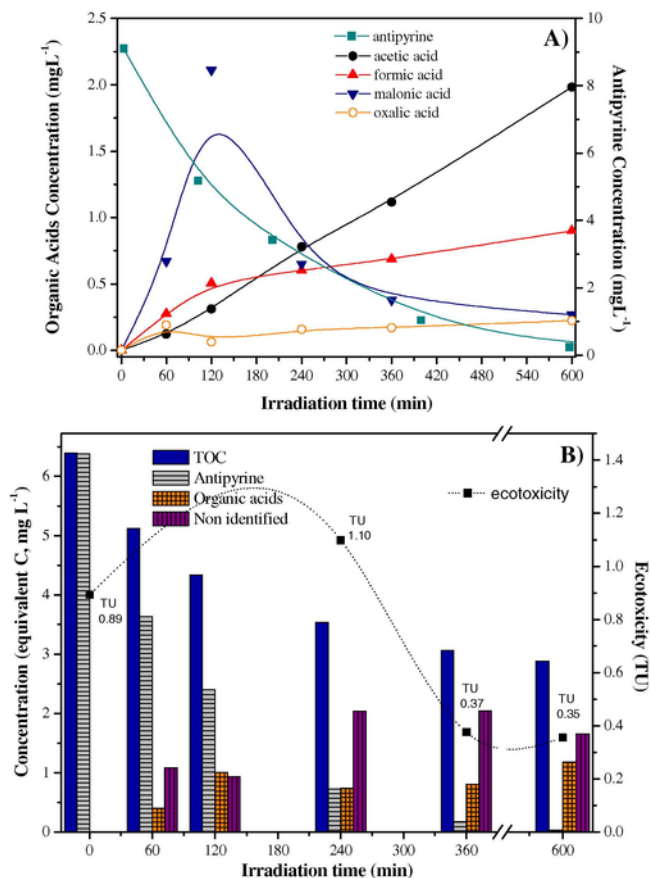


Fig. 9. A) Time-course of ANT and organic acids upon solar irradiation with the $\text{TiO}_2\text{-0.5ZnO/cloi}$ photocatalyst; B) evolution of the ecotoxicity (TU), measured TOC and TOC corresponding to non-identified by-products.

3.2.6. Experiments with scavengers

The basis of the photo-induced processes is well known. A semiconductor can be excited by light energy higher than the band gap inducing the formation of electron-hole pairs, which can transfer charge to adsorbed species on the semiconductor surface by forming radicals that oxidize organic chemicals. The role of the oxidizing entities can be qualitatively assessed by using quenching agents that can trap different radicals and holes, causing partial suppression of the reaction and the decrease of the rate constant [62,63]. Some radical-trapping experiments were conducted to learn on the role of the main active species. Thus, isopropanol (iPrOH) has been used for quenching $\cdot\text{OH}$, KI as scavenger of both h^+ and $\cdot\text{OH}$ and benzoquinone (BQ) for the superoxide $\text{O}_2^{\cdot-}$ radicals [62,64,65]. Fig. 11 depicts the values of the first-order rate constant of ANT and ACE disappearance (k) with $\text{TiO}_2\text{-0.5ZnO/cloi}$ under solar light using these scavengers. The k values for ACE degradation decreased in the presence of iPrOH , KI and BQ, which suggests that the holes as well as $\cdot\text{OH}$ and $\text{O}_2^{\cdot-}$ radicals are all involved in the oxidation of this compound. These oxidizing entities are also responsible of the degradation of ANT, according to the reduction of k values shown in Fig. 11. Nevertheless, it is important to remark that the decrease caused by KI is quite higher than the observed in presence of the two other scavengers, suggesting that the main contribution to the oxidative degradation of ANT proceeds from h^+ and $\cdot\text{OH}$. Because the photocatalyst used in these experiments is the same, the different behavior of the holes and radicals can be apparently due to the nature of the pollutant. The function of $\text{O}_2^{\cdot-}$ radicals is quite interesting in this process and indicates that O_2 adsorbed

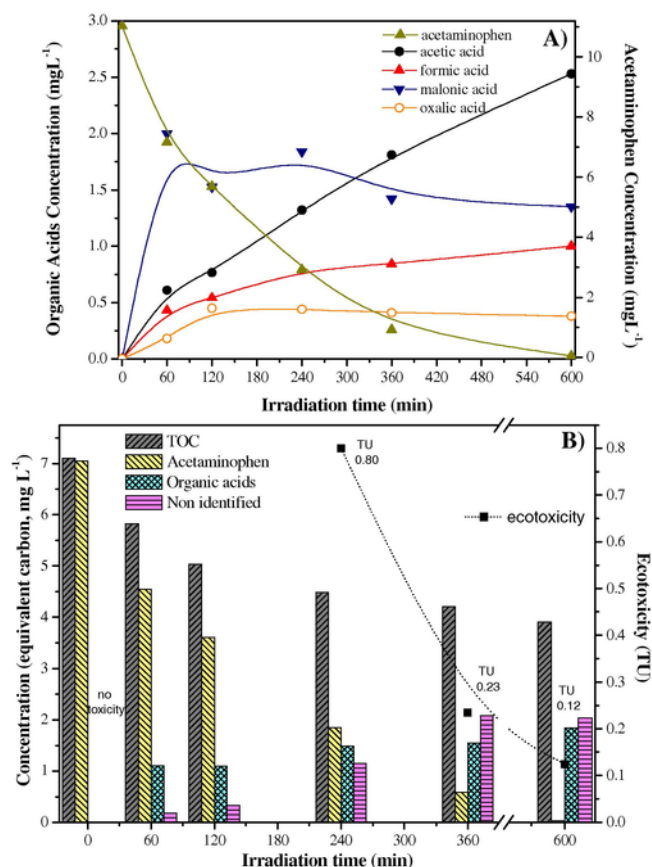


Fig. 10. A) Time-course of ACE and organic acids upon solar irradiation with the $\text{TiO}_2\text{-}0.5\text{ZnO/cloi}$ photocatalyst; B) evolution of the ecotoxicity (TU), measured TOC and TOC corresponding to non-identified by-products.

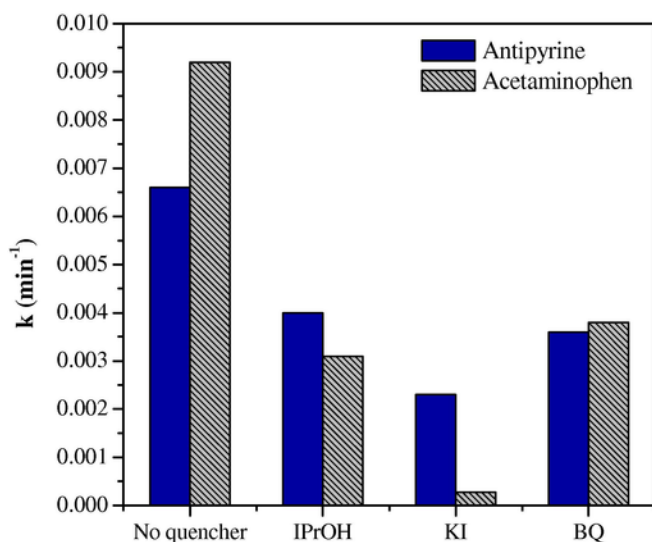


Fig. 11. Values of the first-order rate constant of ACE and ANT disappearance with $\text{TiO}_2\text{-}0.5\text{ZnO/cloi}$ in presence of different scavengers ($[\text{pollutant}]_0 = 10 \text{ mg L}^{-1}$; $[\text{scavenger}] = 0.001 \text{ M}$; $[\text{photocatalyst}] = 250 \text{ mg L}^{-1}$; light intensity = 650 W m^{-2}).

on the surface of the catalyst acts as electron trap, thus preventing the recombination of the photogenerated charges. These results show

that although the highly oxidizing $\cdot\text{OH}$ radicals can oxidize many organic compounds they do not dominate the photodegradation process under solar light with these $\text{TiO}_2\text{-ZnO/clay}$ heterostructures.

4. Conclusions

Novel $\text{TiO}_2\text{-ZnO/clay}$ nanoarchitectures have been prepared by adapting a simple sol-gel method. The methodology allows obtaining in a one-step pathway $\text{TiO}_2\text{-ZnO}$ nanoparticles supported on the surface of a delaminated layered clay. The structural characterization demonstrated that using low ZnO loadings (from 0.2 to 1%) was possible to achieve the crystallization of anatase, without the formation of other undesired phases. Photocatalytic activity tests showed that $\text{TiO}_2\text{-ZnO/cloisite}$ with 0.5% of ZnO presents the best performance for acetaminophen and antipyrine degradation under solar light. This benefit derives from the heterojunction between $\text{TiO}_2\text{-ZnO}$ semiconductors and a delaminated layered clay that reduces the electron-hole recombination. ANT showed higher degradation rate than ACE. In both cases the degradation was enhanced at low concentrations and increasing irradiation intensity. Almost complete conversion of both target compounds was achieved after 10 h but accompanied by less than 50% TOC reduction. The remaining TOC corresponded in about one-half to short-chain organic acids, mainly acetic. The rest of organic carbon was in non-identified species with very low significance in terms of ecotoxicity given the low ecotoxicity values of the samples from the photocatalytic treatment. The photocatalyst also showed a remarkable stability after four operation cycles. Experiments with radical scavengers suggest that the degradation of both pharmaceuticals involves the action of holes, $\cdot\text{OH}$ and $\text{O}_2^{\cdot-}$, although the superoxide radical plays a less important role in the case of antipyrine.

Acknowledgements

The authors acknowledge the financial support from Spanish MINECO (project CTQ2013-41963-R). C.B. is indebted to the MINECO for a Ramon y Cajal postdoctoral contract. Thanks to Dr. Gamarra and the SAIUEX service for the TEM characterization.

Appendix A. Supplementary data

Supplementary data associated with this article can be found, in the online version, at <http://dx.doi.org/10.1016/j.cej.2016.10.002>.

References

- [1] R. Loos, B.M. Gawlik, G. Locoro, E. Rimaviciute, S. Contini, G. Bidoglio, Eu-wide survey of polar organic persistent pollutants in European river waters, *Environ. Pollut.* 157 (2009) 561–568.
- [2] P. Amrita, K. Yew-Hoong Gin, A. Yu-Chen Lin, M. Reinhard, Impacts of emerging contaminants on freshwater resources: review of recent occurrences, sources, fate and effects, *Sci. Total Environ.* 408 (2010) 6062–6069.
- [3] R. Loos, G. Locoro, S. Comero, S. Contini, D. Schwesig, F. Werres, P. Balsaa, O. Gans, S. Weiss, L. Blaha, M. Bolchi, B.M. Gawlik, Pan-European survey on the occurrence of selected polar organic persistent pollutants in ground water, *Water Res.* 44 (2010) 4115–4126.
- [4] Q. Sun, M. Lv, A. Hu, X. Yang, C.P. Yu, Seasonal variation in the occurrence and removal of pharmaceuticals and personal care products in a wastewater treatment plant in Xiamen, China, *J. Hazard. Mater.* 277 (2014) 69–75.
- [5] M. Tobajas, V. Verdugo, A.M. Polo, J.J. Rodriguez, A.F. Mohedano, Assessment of toxicity and biodegradability on activated sludge of priority and emerging pollutants, *Environ. Technol.* 37 (2016) 713–721.
- [6] K. Xia, A. Bhandari, K. Das, G. Pillar, Occurrence and fate of pharmaceuticals and personal care products (PPCPs) in biosolids, *J. Environ. Qual.* 34 (2005) 91–104.

- [7] N. Klammerth, S. Malato, M.I. Maldonado, A. Agüera, A.R. Fernandez-Alba, Application of photo-Fenton as tertiary treatment of emerging contaminants in municipal wastewater, *Environ. Sci. Technol.* 44 (2010) 1792–1798.
- [8] M. Petrovic, S. Gonzalez, D. Barcelo, Analysis and removal of emerging contaminants in wastewater and drinking water, *TrAC Trends Anal. Chem.* 22 (2003) 685–696.
- [9] Y. Liu, K. Wan, N. Deng, F. Wu, Photodegradation of paracetamol in montmorillonite KSF suspension, *React. Kinet. Mech. Catal.* 99 (2010) 493–502.
- [10] I.M. Sebastine, R.J. Wakeman, Consumption and environmental hazards of pharmaceutical substances in the UK, *Process Saf. Environ.* 81 (2003) 229–235.
- [11] X. Zhang, F. Wu, X.W. Wu, P. Chen, N. Deng, Photodegradation of acetaminophen in TiO_2 suspended solution, *J. Hazard. Mater.* 157 (2008) 300–307.
- [12] J.S.N. Muir, J.D. Nichols, M.R. Stillings, The influence of dosage form on aspirin kinetics: implications for acute cardiovascular use, *Curr. Med. Res. Opin.* 13 (1997) 491–500.
- [13] D.W. Kolpin, E.T. Furlong, M.T. Meyer, E.M. Thurman, S.D. Zaugg, L.B. Barber, H.T. Buxton, Pharmaceuticals, hormones, and other organic wastewater contaminants in US streams, 1999–2000: a national reconnaissance, *Environ. Sci. Technol.* 36 (2002) 1202–1211.
- [14] P.H. Roberts, K.V. Thomas, The occurrence of selected pharmaceuticals in wastewater effluent and surface waters of the lower Tyne catchment, *Sci. Total Environ.* 356 (2006) 143–153.
- [15] T. Ternes, Occurrence of drugs in German sewage treatment plants and rivers, *Water Res.* 32 (1998) 3245–3260.
- [16] A. Ziyilan-Yavas, Y. Mizukoshi, Y. Maeda, N.H. Ince, Supporting of pristine TiO_2 with noble metals to enhance the oxidation and mineralization of paracetamol by sonolysis and sonophotolysis, *Appl. Catal. B* 172–173 (2015) 7–17.
- [17] T. Deblonde, C. Cossu-Leguille, P. Hartemann, Emerging pollutants in wastewater: a review of the literature, *Int. J. Hyg. Environ. Health* 214 (2011) 442–448.
- [18] V. Sarriá, S. Parra, N. Adler, P. P. ringer, N. Benitez, C. Pulgarín, Recent developments in the coupling of photoassisted and aerobic biological processes for the treatment of biorecalcitrant compounds, *Catal. Today* 76 (2002) 301–315.
- [19] S. Sanchis, A.M. Polo, M. Tobajas, J.J. Rodríguez, A.F. Mohedano, Coupling Fenton and biological removal of nitrochlorinated herbicides from water, *Water Res.* 49 (2014) 197–206.
- [20] C.-T. Chang, J.-J. Wang, T. Ouyang, Q. Zhang, Y.-H. Jing, Photocatalytic degradation of acetaminophen in aqueous solutions by TiO_2 /ZSM-5 zeolite with low energy irradiation, *Mater. Sci. Eng. B* 196 (2015) 53–60.
- [21] J. Radjenovic, C. Sirtori, M. Petrovic, D. Barceló, S. Malato, Solar photocatalytic degradation of persistent pharmaceuticals at pilot-scale: kinetics and characterization of major intermediate products, *Appl. Catal. B* 89 (2009) 255–264.
- [22] A. Duran, J.M. Monteagudo, I. Sanmartín, A. Carrasco, Solar photo-Fenton mineralization of antipyrine in aqueous solution, *J. Environ. Manage.* 130 (2013) 64–71.
- [23] O. Gonzalez, C. Sans, S. Esplugas, Sulfamethoxazole abatement by photo-Fenton toxicity, inhibition and biodegradability assessment of intermediates, *J. Hazard. Mater.* 146 (2007) 459–464.
- [24] S. Malato, J. Blanco, D.C. Alarcón, M.I. Maldonado, P. Fernández-Ibáñez, W. Germjak, Photocatalytic decontamination and disinfection of water with solar collectors, *Catal. Today* 122 (2007) 137–149.
- [25] L. Liu, X. Chen, Titanium dioxide nanomaterials: self-structural modifications, *Chem. Rev.* 114 (2014) 9890–9918.
- [26] S. Rehman, R. Ullah, A.M. Butt, N.D. Gohar, Strategies of making TiO_2 and ZnO visible light active, *J. Hazard. Mater.* 170 (2009) 560–569.
- [27] J. Herrmann, Heterogeneous photocatalysis: fundamentals and applications to the removal of various types of aqueous pollutants, *Catal. Today* 53 (2005) 115–129.
- [28] Y. Zhang, D. Wang, G. Zhang, Photocatalytic degradation of organic contaminants by TiO_2 /sepiolite composites prepared at low temperature, *Chem. Eng. J.* 173 (2011) 1–10.
- [29] Y. Zhang, Z. Jiang, J. Huang, L.Y. Lim, W. Li, J. Deng, D. Gong, Y. Tang, Y. Lai, Z. Chen, Titanate and titania nanostructured materials for environmental and energy applications: a review, *RSC Adv.* 5 (2015) 79479–79510.
- [30] H. Wang, L. Zhang, Z. Chen, J. Hu, S. Li, Z. Wang, J. Liu, X. Wang, Semiconductor heterojunction photocatalysts: design, construction, and photocatalytic performances, *Chem. Soc. Rev.* 43 (2014) 5234–5244.
- [31] M. Pelaez, N.T. Nolan, S.C. Pillai, M.K. Seery, P. Falaras, A.G. Kontos, P.S.M. Dunlop, J.W.J. Hamilton, J.A. Byrne, K. O'Shea, M.H. Entezari, D.D. Dionysiou, A review on the visible light active titanium dioxide photocatalysts for environmental applications, *Appl. Catal. B* 125 (2012) 331–349.
- [32] L. Pan, G.-Q. Shen, J.-W. Zhang, X.-C. Wei, L. Wang, J.-J. Zou, X. Zhang, TiO_2 -ZnO composite sphere decorated with ZnO clusters for effective charge isolation in photocatalysis, *Ind. Eng. Chem. Res.* 54 (2015) 7226–7232.
- [33] M. Kwiatkowski, I. Bezverkhyy, M. Skompskab, ZnO nanorods covered with a TiO_2 layer: simple sol-gel preparation, and optical, photocatalytic and photoelectrochemical properties, *J. Mater. Chem. A* 3 (2015) 12748–12760.
- [34] X. Zheng, D. Li, X. Li, J. Chen, C. Cao, J. Fang, J. Wang, Y. He, Y. Zheng, Construction of ZnO/TiO_2 photonic crystal heterostructures for enhanced photocatalytic properties, *Appl. Catal. B* 168–169 (2015) 408–415.
- [35] J.H. Pan, H. Dou, Z. Xiong, C. Xu, J. Ma, X.S. Zhao, Porous photocatalysts for advanced water purifications, *J. Mater. Chem.* 20 (2010) 4512–4528.
- [36] J. Chen, F. Qiu, W. Xu, S. Cao, H. Zhu, Recent progress in enhancing photocatalytic efficiency of TiO_2 -based materials, *Appl. Catal. A* 495 (2015) 131–140.
- [37] M.N. Chong, B. Jin, C.W.K. Chow, C. Saint, Recent developments in photocatalytic water treatment technology: a review, *Water Res.* 44 (2010) 2997–3027.
- [38] M. Ge, C. Cao, J. Huang, S. Li, Z. Chen, K.-Q. Zhang, S.S. Al-Deyab, Y. Lai, A review of one-dimensional TiO_2 nanostructured materials for environmental and energy applications, *J. Mater. Chem. A* 4 (2016) 6772–6801.
- [39] C. Yu, W. Zhou, H. Liu, Y. Liu, D.D. Dionysiou, Design and fabrication of microsphere photocatalysts for environmental purification and energy conversion, *Chem. Eng. J.* 287 (2016) 117–129.
- [40] K. Rajeshwar, W. Chanmanee, Bioinspired photocatalyst assemblies for environmental remediation, *Electrochim. Acta* 84 (2012) 96–102.
- [41] T. Kaneko, H. Shimotsuma, M. Kajikawa, T. Hatamachi, T. Kodama, Y. Kityayama, Synthesis and photocatalytic activity of titania pillared clays, *J. Porous Mater.* 8 (2001) 295–301.
- [42] K. Sahel, M. Bouhent, F. Belkhadem, C. Guillard, F. Figueras, Photocatalytic degradation of anionic and cationic dyes over TiO_2 P25, and Ti-pillared clays and Ag-doped Ti-pillared clays, *Appl. Clay Sci.* 95 (2014) 205–210.
- [43] S. Yang, G. Liang, A. Gu, H. Mao, Synthesis of TiO_2 pillared montmorillonite with ordered interlayer mesoporous structure and high photocatalytic activity by an intra-gallery templating method, *Mater. Res. Bull.* 48 (2013) 3948–3954.
- [44] J. Liu, G. Zhang, Recent advances in synthesis and applications of clay-based photocatalysts: a review, *Phys. Chem. Chem. Phys.* 16 (2014) 8178–8192.
- [45] C. Belver, J. Bedia, J.J. Rodriguez, Titania-clay heterostructures with solar photocatalytic applications, *Appl. Catal. B* 176–177 (2015) 278–287.
- [46] P. Aranda, C. Belver, E. Ruiz-Hitzky, Inorganic heterostructured materials based on clay minerals, in: L.F. Drummy, M. Ogawa, P. Aranda (Eds.), *Materials and Clay Minerals*, CMS Workshop Series, vol. 18, The Clay Minerals Society, 2013.
- [47] C. Belver, J. Bedia, M.A. Álvarez-Montero, J.J. Rodriguez, Solar photocatalytic purification of water with Ce-doped TiO_2 /clay heterostructures, *Catal. Today* 266 (2016) 36–45.
- [48] C. Belver, P. Aranda, M.A. Martín-Luengo, E. Ruiz-Hitzky, New silica/alumina-clay heterostructures: properties as acid catalysts, *Microporous Mesoporous Mater.* 147 (2012) 157–166.
- [49] J. Tauc, Absorption edge and internal electric fields in amorphous semiconductors, *Mater. Res. Bull.* 5 (1970) 721–726.
- [50] J. Zhang, P. Zhou, J. Liu, J. Yu, New understanding of the difference of photocatalytic activity among anatase, rutile and brookite TiO_2 , *Phys. Chem. Chem. Phys.* 16 (2014) 20382–20386.
- [51] J. Brinker, G.W. Scherer, C.J. Brinker, *Sol-Gel Science: The Physics and Chemistry of Sol-Gel Processing*, Academic Press, Oxford, 1990.
- [52] E. Ruiz-Hitzky, P. Aranda, C. Belver, Nanoarchitectures based on clay materials, in: K. Ariga (Ed.), *Manipulation on Nanoscale Materials: An Introduction to Nanoarchitectonics*, The Royal Society of Chemistry, Cambridge, 2012, pp. 87–111.
- [53] A. Gil, S.A. Korili, M.A. Vicente, Recent advances in the synthesis and catalytic applications of pillared clays, *Catal. Rev.* 50 (2008) 153–221.
- [54] O. Carp, C.L. Huisman, A. Reller, Photoinduced reactivity of titanium dioxide, *Prog. Solid State Chem.* 32 (2004) 33–177.
- [55] M. Anpo, M. Takeuchi, The design and development of highly reactive titanium oxide photocatalysts operating under visible light irradiation, *J. Catal.* 216 (2003) 505–516; M. Anpo, Preparation, characterization, and reactivities of highly functional titanium oxide-based photocatalysts able to operate under UV-visible light irradiation: approaches in realizing high efficiency in the use of visible light, *Bull. Chem. Soc. Jpn.* 77 (2004) 1427–1442.

- [56] M.A. Butler, Photoelectrolysis and physical properties of the semiconducting electrode WO_3 , *J. Appl. Phys.* 48 (1977) 1914–1920.
- [57] M.H. Habibi, A. Hassanzadeh, S. Mahdavi, The effect of operational parameters on the photocatalytic degradation of three textile azo dyes in aqueous TiO_2 suspensions, *J. Photochem. Photobiol. A* 172 (2005) 895–898.
- [58] N. Serpone, Relative photonic efficiencies and quantum yields in heterogeneous photocatalysis, *J. Photochem. Photobiol. A* 104 (1997) 1–12.
- [59] F. Yuan, Ch. Hu, X. Hu, J. Qu, M. Yang, Degradation of selected pharmaceuticals in aqueous solution with UV and UV/ H_2O_2 , *Water Res.* 43 (2009) 1766–1774.
- [60] E. Moctezuma, E. Leyva, C.A. Aguilar, R.A. Luna, C. Montalvo, Photocatalytic degradation of paracetamol: intermediates and total reaction mechanism, *J. Hazard. Mater.* 243 (2012) 130–138.
- [61] L. Yang, L.E. Yu, M.B. Ray, Degradation of paracetamol in aqueous solutions by TiO_2 photocatalysis, *Water Res.* 42 (2008) 3480–3488.
- [62] G. Li, K.H. Wong, X. Zhang, C. Hu, J.C. Yu, R.C.Y. Chan, P.K. Wong, Degradation of acid Orange 7 using magnetic AgBr under visible light: the roles of oxidizing species, *Chemosphere* 76 (2009) 1185–1191.
- [63] W. Li, D. Li, Y. Lin, P. Wang, W. Chen, X. Fu, Y. Shao, Evidence for the active species involved in the photodegradation process of methyl orange on TiO_2 , *J. Phys. Chem.* 116 (2012) 3552–3560.
- [64] S. Chen, Y. Hu, S. Meng, X. Fu, Study on the separation mechanisms of photo-generated electrons and holes for composite photocatalysts g- C_3N_4 - WO_3 , *Appl. Catal. B* 150–151 (2014) 564–573.
- [65] Y.X. Chen, S.Y. Yang, K. Wang, L.P. Lou, Role of primary active species and TiO_2 surface characteristic in UV-illuminated photodegradation of acid orange 7, *J. Photochem. Photobiol. A* 172 (2005) 47–54.